CellPress

Developmental Cell
Article

Decoy Receptor CXCR7 Modulates Adrenomedullin-Mediated Cardiac and Lymphatic Vascular Development

Klara R. Klein,[1] Natalie O. Karpinich,[1] Scott T. Espenschied,[1] Helen H. Willcockson,[1] William P. Dunworth,[2] Samantha L. Hoopes,[1] Erich J. Kushner,[3] Victoria L. Bautch,[3] and Kathleen M. Caron[1,2,*]
[1]Department of Cell Biology and Physiology, The University of North Carolina, Chapel Hill, NC 27599, USA
[2]Department of Genetics, The University of North Carolina, Chapel Hill, NC 27599, USA
[3]Department of Biology, The University of North Carolina, Chapel Hill, NC 27599, USA
*Correspondence: kathleen_caron@med.unc.edu
http://dx.doi.org/10.1016/j.devcel.2014.07.012

SUMMARY

Atypical 7-transmembrane receptors, often called decoy receptors, act promiscuously as molecular sinks to regulate ligand bioavailability and consequently temper the signaling of canonical G protein-coupled receptor (GPCR) pathways. Loss of mammalian CXCR7, the most recently described decoy receptor, results in postnatal lethality due to aberrant cardiac development and myocyte hyperplasia. Here, we provide the molecular underpinning for this proliferative phenotype by demonstrating that the dosage and signaling of adrenomedullin (*Adm*, gene; AM, protein)—a mitogenic peptide hormone required for normal cardiovascular development—is tightly controlled by CXCR7. To this end, *Cxcr7*$^{-/-}$ mice exhibit gain-of-function cardiac and lymphatic vascular phenotypes that can be reversed upon genetic depletion of adrenomedullin ligand. In addition to identifying a biological ligand accountable for the phenotypes of *Cxcr7*$^{-/-}$ mice, these results reveal a previously underappreciated role for decoy receptors as molecular rheostats in controlling the timing and extent of GPCR-mediated cardiac and vascular development.

INTRODUCTION

The precise spatiotemporal dosage of mitogenic and chemotactic factors is critical for the proper organization and development of organ systems. While the concentration of ligands often differs between tissues and developmental stages, the bioavailability of ligands within local microenvironments must also be controlled at a cellular level. Thus, cells can express molecular sink receptors, which in an autocrine or paracrine manner, sequester ligand away from canonical signaling receptors, thereby driving important developmental processes like neurogenesis, angiogenesis, chemotaxis, and cellular proliferation (Graham et al., 2012; Nibbs and Graham, 2013). Molecular sink receptors include atypical chemokine receptors, also known as decoy receptors, which belong to the larger family of 7-transmembrane receptors. Decoy receptors act as molecular sinks by binding, internalizing, and degrading a wide range of ligands independent of G protein coupling (Graham et al., 2012). CXCR7 is the most recently described decoy receptor and has been extensively studied for its role as a CXCL12/SDF-1 receptor (Boldajipour et al., 2008; Naumann et al., 2010; Thelen and Thelen, 2008), particularly in tumor cell migration and cancer progression (Duda et al., 2011; Sánchez-Martín et al., 2013).

However, prominent roles for CXCR7 during normal development and physiology have also been recently appreciated. In zebrafish, the expression and molecular sink functions of CXCR7 in trailing cells of the posterior lateral line primordium allow for a CXCL12 chemotactic gradient to be established and sensed by the leading primordial germ cells that express CXCR4, the canonical SDF-1/CXCL12 receptor (Dambly-Chaudière et al., 2007; Donà et al., 2013; Valentin et al., 2007; Venkiteswaran et al., 2013). In this instance, CXCR7 exerts its decoy activities over a wide region to help coordinate and guide the migration of multicellular tissue structures.

However, the decoy activities of CXCR7 can also occur in a cell-autonomous fashion. For example, the coexpression of CXCR7 within migrating cortical neurons allows for the continued sensitization and chemotactic signaling of CXCR4—rather than receptor desensitization and downregulation that would typically occur within an environment of high CXCL12 ligand (Sánchez-Alcañiz et al., 2011; Wang et al., 2011). Recently, CXCR7 expression in endothelial cells has also been shown to regulate circulating levels of ligands, suggesting that CXCR7 expression in vessels may not only affect signaling events in a microenvironment, but systemically as well (Berahovich et al., 2014).

Due to these well-described roles in the CXCL12/CXCR4 signaling axis, *Cxcr7*$^{-/-}$ mice were expected to exhibit phenotypes that might resemble gain-of-function mutations for the CXCL12/CXCR4 signaling axis. However, *Cxcr7*$^{-/-}$ mice have unexpected phenotypes including cardiomyocyte hyperplasia and postnatal lethality associated with gross cardiac enlargement and cardiac valve defects (Gerrits et al., 2008; Sierro et al., 2007; Yu et al., 2011). Because decoy receptors typically bind and sequester multiple ligands, it has been difficult to discern which ligand may be causally related to the developmental cardiac defects of *Cxcr7*$^{-/-}$ mice. In this regard, we

appreciated that CXCR7 was originally identified as RDC1—a putative receptor for adrenomedullin (*Adm*, gene; AM, protein), a 52 amino acid mitogenic peptide hormone critical for cardiac and lymphatic vascular development (Caron and Smithies, 2001; Dackor et al., 2006; Dunworth et al., 2008; Fritz-Six et al., 2008). AM binds RDC1/CXCR7 with a K_d of 1.9 × 10^{-7} M, similar to CLR when associated with RAMPs (Kapas and Clark, 1995). Importantly, we have recently shown that genetic overexpression of AM ligand in $Adm^{hi/hi}$ mice results in gross cardiac enlargement due to cardiac hyperplasia during embryogenesis (Wetzel-Strong et al., 2014), which closely phenocopies the dysmorphic cardiac hyperplasia of $Cxcr7^{-/-}$ mice.

We therefore sought to address whether a principal function of CXCR7 may involve controlling the dosage of AM ligand during development, first focusing our attention on the cardiac hyperplasia. In the course of our studies, we also discovered lymphatic vascular defects in $Cxcr7^{-/-}$ mice, which are consistent with the prominent role that AM signaling plays in driving normal lymphangiogenesis (Dunworth et al., 2008; Fritz-Six et al., 2008; Hoopes et al., 2012; Karpinich et al., 2011). In addition to identifying a biological ligand that is causally associated with the $Cxcr7^{-/-}$ phenotypes, the results described here elucidate a role for decoy receptors as molecular rheostats that control normal cardiac and lymphatic vascular development.

RESULTS

Gene Expression of *Cxcr7* and *Adm* Are Coupled in the Heart and Lymphatic Endothelium

Historical ligand binding data (Kapas and Clark, 1995) and more recent findings show a downregulation of *Adm* gene expression in $Cxcr7^{-/-}$ mice (Sierro et al., 2007) and strongly support the existence of this ligand-receptor pair. Considering the well-established function of CXCR7 as a decoy receptor, we predicted that expression levels of *Cxcr7* may homeostatically increase under conditions of increased AM peptide. To further evaluate whether this interaction exists, we measured the expression of *Cxcr7* in hearts of $Adm^{hi/hi}$ mice which have a genetically engineered, 3-fold increase in *Adm* gene expression (Wetzel-Strong et al., 2014). Indeed, utilizing quantitative real-time PCR (qRT-PCR), we identified a potent 2.5-fold upregulation of *Cxcr7* gene expression in $Adm^{hi/hi}$ cardiac tissue compared to that of wild-type littermates (Figure 1A). Conversely, loss of *Adm* expression in isolated endothelial cells resulted in a nearly 5-fold reduction in *Cxcr7* expression (Figure 1A).

We also found that *Cxcr7* is expressed at high levels in isolated, adult lymphatic vessels—a tissue where AM peptide plays important roles (Figure S1A available online). Consistently, microarray analysis of cultured, human lymphatic endothelial cells (LECs) showed that expression of the human *CXCR7* gene (aka *ACKR3* or *CMKOR1*) was one of the ten most significantly induced genes within 1 hr of 10 nM AM treatment (p = 2.5E–07) (Figure 1B; Table S1). This finding was further confirmed by qRT-PCR, revealing a 4-fold increase in *CXCR7* gene expression following 1 hr and 24 hr of AM treatment (Figure 1C). Pretreatment with $AM_{22–52}$, a CLR/R2 antagonist, significantly reduced this AM-mediated increase (Figure 1C), demonstrating that the upregulation of *CXCR7* gene expression is modulated through the canonical AM receptor. Collectively, these data indicate that *CXCR7* and *ADM* gene expression levels are coupled within tissues where AM peptide plays important developmental and physiological roles. Because excess AM, either by genetic overexpression in vivo or exogenous treatment in vitro, triggered an increase in *CXCR7* expression, we next tested directly the hypothesis that CXCR7 serves as a decoy receptor to modify AM concentration.

CXCR7 Scavenges AM Peptide and Dampens Canonical AM Signaling

Using a classical scavenger assay, CXCR7-expressing HEK293T cells were treated with biotinylated-$AM^{1–52}$, and aliquots of media were collected over time to determine the remaining levels of AM peptide within the media. While the levels of biotinylated-$AM^{1–52}$ in the media of vector-transfected control cells remained unchanged, CXCR7-expressing cells rapidly and steadily depleted AM peptide from the media to levels that were statistically lower than control cells by the conclusion of the time course (Figures 1D and 1E). These data demonstrate the ability of CXCR7 to modulate AM ligand concentrations exogenously in a controlled in vitro system.

To determine whether this scavenging of AM peptide by CXCR7 was conserved in vivo, we compared AM staining in cardiac tissue of wild-type mice and $Cxcr7^{-/-}$ mice, which harbor an insertional GFP reporter within the targeted allele. First, we noted that expression of the GFP reporter was enriched within the epicardium and the endocardium surrounding the trabeculae and weakly expressed in the compact zone (Figure 1F). Second, the staining pattern of receptor expression was spatially juxtaposed and/or overlapping with the most prominent sites of AM peptide expression, including the epicardium and trabeculae (Figure 1G) (Wetzel-Strong et al., 2014). Remarkably, we found a significant 30% increase in the relative staining intensities of AM peptide in the epicardium and trabeculae of $Cxcr7^{-/-}$ mice compared to wild-type littermates (Figures 1H–1K), but no changes within the compact zone where levels of *Cxcr7* reporter expression were modest (Figure 1L). These findings indicate that spatially juxtaposed and/or overlapping expression of CXCR7 and AM during cardiac development is essential for scavenging AM peptide in cardiac tissue in vivo.

Activation of the canonical AM-receptor complex, CLR and receptor activity modifying protein 2 (RAMP2), elicits an increase in cAMP and subsequent downstream activation and phosphorylation of ERK (Fritz-Six et al., 2008). Utilizing a highly sensitive bioluminescence resonance energy transfer (BRET) reporter system (Barak et al., 2008; Ponimaskin et al., 2007), we found that HEK293T cells that overexpress CXCR7 failed to accumulate cAMP upon AM stimulation—a finding consistent with the lack of G protein coupling by decoy receptors (Figure S1B). As expected, AM treatment of CLR/RAMP2-expressing cells resulted in a potent accumulation of cAMP (Figure S1B) and pERK:tERK upregulation (Figures 1M, 1N, and S1C). Importantly, while AM did not elicit a pERK:tERK upregulation in cells transfected with *CXCR7* alone, the CLR-RAMP2-mediated activation of pERK:tERK was markedly abrogated when cells were cotransfected with *CXCR7* (Figures 1M and 1N). These in vitro signaling assays demonstrate that CXCR7 can act as a

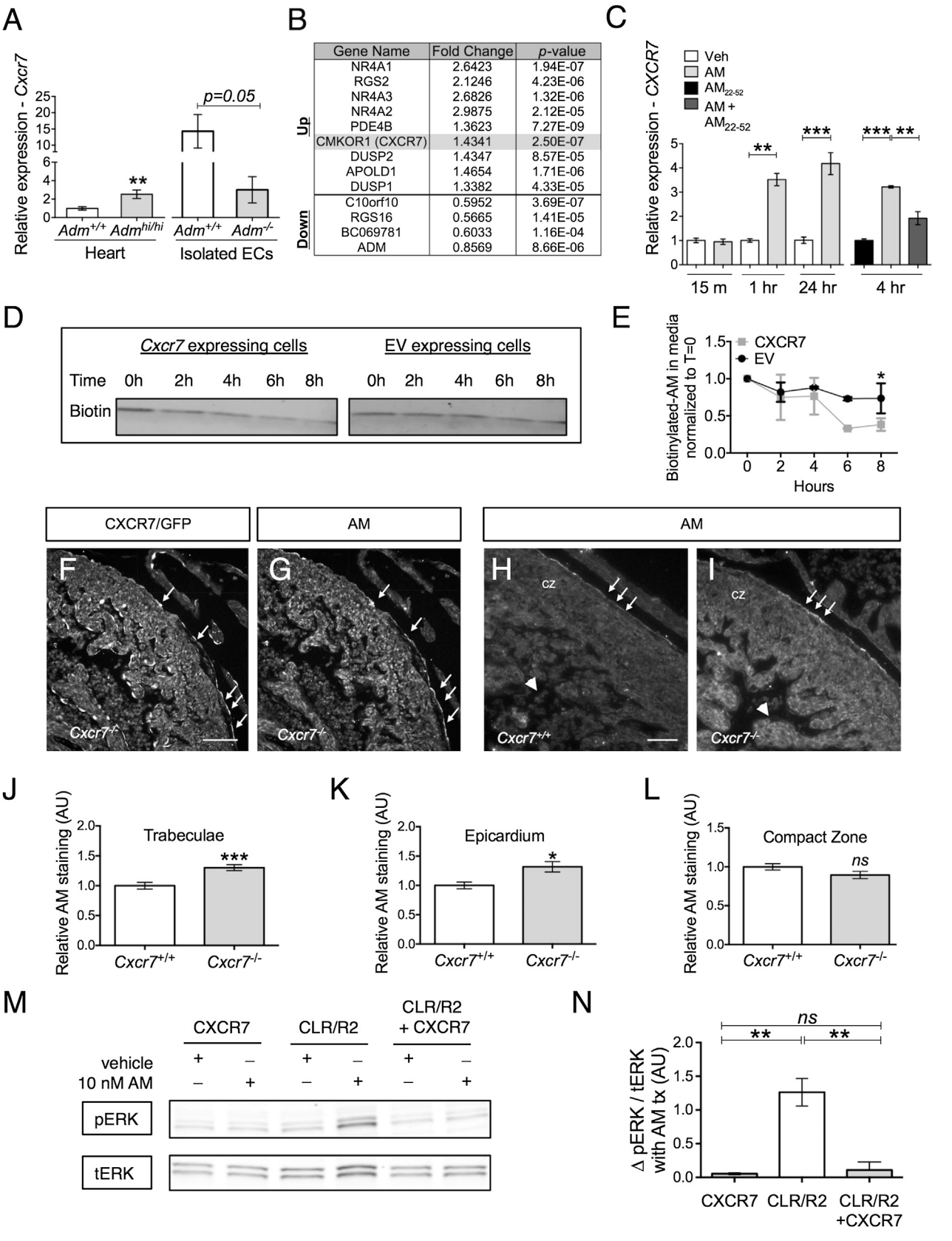

(legend on next page)

cell-autonomous molecular rheostat to dampen canonical AM pERK:tERK signaling.

The effects of CXCR7 on dampening pERK:tERK signaling were also confirmed in vivo, where we noted significant accumulation of pERK staining in dermal lymphatic vessels of postnatal day 1 *Cxcr7*$^{-/-}$ tail skin compared to wild-type littermates (Figures S2A–S2D). Furthermore, we also observed a significant increase in the pERK staining in the lymphatic sac of E13.5 *Cxcr7*$^{-/-}$ embryos compared to wild-type animals (Figures S2E–S2J). These in vivo data from a genetic loss-of-function model aptly reciprocate the findings from the in vitro gain-of-function experiments and furthermore demonstrate that loss of *Cxcr7* expression influences ERK phosphorylation on a tissue level.

Cxcr7 Is Dynamically Expressed in Lymphatic Endothelium during Development

Previous studies have reported that nearly one third of adult dermal lymphatic vessels express *CXCR7* (Neusser et al., 2010), but the spatiotemporal expression of *CXCR7* during developmental lymphangiogenesis has yet to be described. Using the GFP-targeted *Cxcr7*$^{+/-}$ reporter allele, we found *Cxcr7* expression colocalized with the lymphatic markers LYVE1 (Figures 2A–2C), Prox1 (Figures 2G–2I), and podoplanin (Figures 2I–2L). At E11.5, lymphatic progenitor cells are arranged in a stereotypically-polarized fashion within the jugular vein (JV) and express *Cxcr7* (Figures 2A–2F, white arrows, 2I, and 2L). Interestingly, we often noted that *Cxcr7* expression is temporarily reduced as the lymphatic progenitors begin to migrate away from the JV (Figures 2F and 2I, asterisks)—underscoring the dynamic expression of the decoy receptor in areas of active cell migration. As lymphatic cells coalesce to form the lymph sacs (LS) between E11.5–E13.5, *Cxcr7* was again expressed in some lymphatics, which were identified by LYVE1 and podoplanin colabeling (Figures 2J–2O). *Cxcr7* was also persistently expressed in the JV cells directly adjacent to the LS (Figures 2P–2R, white arrowheads), consistent with recently published studies demonstrating a paracrine function for decoy receptors (Moissoglu et al., 2014; Venkiteswaran et al., 2013). In summary, *Cxcr7* is highly and dynamically expressed within lymphatic progenitors and early lymphatic vessels at the time of nascent lymphangiogenesis, which also spatiotemporally correlates with the proliferative effects of AM during lymphatic development.

Cxcr7$^{-/-}$ Mice Have Enlarged, Blood-Filled Lymphatic Sacs

We have previously established that AM signaling is required for normal LEC proliferation at E13.5 (Fritz-Six et al., 2008). Thus, we investigated whether loss of *Cxcr7*, which we hypothesize to be a molecular rheostat for AM, disrupts lymphangiogenesis at this point during embryogenesis. Indeed, ~10% of *Cxcr7*$^{-/-}$ mice exhibited visible interstitial edema upon dissection at midgestation (Figures 3A, white arrows, 3B, and 3C, black arrows). Histological evaluation further revealed that ~10%–15% of *Cxcr7*$^{-/-}$ mice displayed interstitial edema, particularly within the thoracic regions surrounding the developing jugular lymphatics. Additionally, we noticed abnormal LS morphology, including markedly enlarged and dysmorphic LS in *Cxcr7*$^{-/-}$ embryos compared to wild-type littermate embryos (Figures 3D–3F). Utilizing computerized morphometry to calculate LS and JV area, we found that the LS:JV ratio of null mice was increased 4-fold compared to *Cxcr7*$^{+/+}$ mice (Figure 3G). Some sections revealed failure of the LS to separate from the JV, with prominent platelet thrombi (Figure 3F, black arrows). Moreover, *Cxcr7*$^{-/-}$ lymphatic vessels exhibited remarkable blood (Figure 3E, asterisks) and proteinaceous deposits (Figure 3E, arrowheads), which are phenotypes commonly ascribed to pathologic lymphangiogenesis and lymph stasis in several mouse models (Bertozzi et al., 2010; Murtomaki et al., 2013). A scoring rubric to assess the severity of lymphatic defects showed that LS of *Cxcr7*$^{-/-}$ embryos had significantly more blood and protein accumulation compared to control mice (Figures 3H and 3I). Taken together, these results demonstrate that loss of *Cxcr7* during embryonic development results in aberrant LS formation.

To determine whether the blood accumulation in the LS was due to improper development or structure of the lymphovenous valves, we stained frontally sectioned embryos with the lymphatic markers Prox1 and podoplanin. We observed no structural differences between *Cxcr7*$^{+/+}$ and *Cxcr7*$^{-/-}$ lymphovenous valves (Figures S3A and S3B), with both wild-type and mutant animals exhibiting characteristic high-Prox1 staining on the valve leaflet. We next considered whether the blood accumulation in *Cxcr7*$^{-/-}$ lymph sacs might be associated with precocious development of the lymphatic sac. As expected, E11.5 wild-type embryos exhibited polarization of LYVE1+ lymphatic progenitors within the jugular vein. However, some *Cxcr7*$^{-/-}$ littermate embryos exhibited premature migration of LECs from

Figure 1. CXCR7 Scavenges AM, Dampens AM-Mediated ERK Phosphorylation In Vitro, and Reduces AM Peptide Levels In Vivo

(A) *Cxcr7* expression in cardiac tissue of *Adm*$^{+/+}$ and *Adm*$^{hi/hi}$ mice (n = 6) and isolated endothelial cells of *Adm*$^{+/+}$ and *Adm*$^{-/-}$ mice (n = 3).

(B) The nine most significantly upregulated and four most significantly downregulated genes in human LECs (hLECs) treated with 10 nM AM for 1 hr.

(C) *CXCR7* expression in vehicle and 10 nM AM-treated hLECs at 15 min, 1 hr, and 24 hr, and AM_{22-52}, AM, and [AM_{22-52}+AM] for 4 hr.

(D and E) Representative western blots probed for biotin (D) and quantitation of biotinylated-AM^{1-52} (E) depletion over 8 hr by either CXCR7- or EV-expressing cells in three independent experiments.

(F and G) *Cxcr7* and AM staining in E13.5 *Cxcr7*$^{-/-}$ cardiac tissue with epicardial colocalization (white arrows).

(H and I) AM staining of E13.5 *Cxcr7*$^{+/+}$ and *Cxcr7*$^{-/-}$ cardiac tissue. White arrows highlight epicardium, CZ identifies the compact zone, and white arrowheads highlight the cardiac trabeculae. Images were obtained at the same exposure and the amount of AM expressed in the three regions of the heart was assessed by measuring the integrated density of staining using ImageJ software (n = 3–5). Scale bars represent 100 μM.

(J–L) Quantitation of AM staining intensity in *Cxcr7*$^{+/+}$ (n = 3) versus *Cxcr7*$^{-/-}$ (n = 5) animals in three regions of the heart, trabeculae, epicardium, and compact zone. Staining intensity is expressed as arbitrary units of integrated density as measured by ImageJ.

(M and N) Representative western blot (M) and quantitation of change (N) in pERK:tERK between vehicle and 10 nM AM-treated CXCR7-, CLR/R2-, and CLR/R2+CXCR7-expressing HEK293T. Quantitation was calculated using three independent experiments run on the same gel.

In (A)–(L), data are represented as mean ± SEM. *$p < 0.05$, **$p < 0.01$, ***$p < 0.001$.

See also Figures S1 and S2 and Table S1.

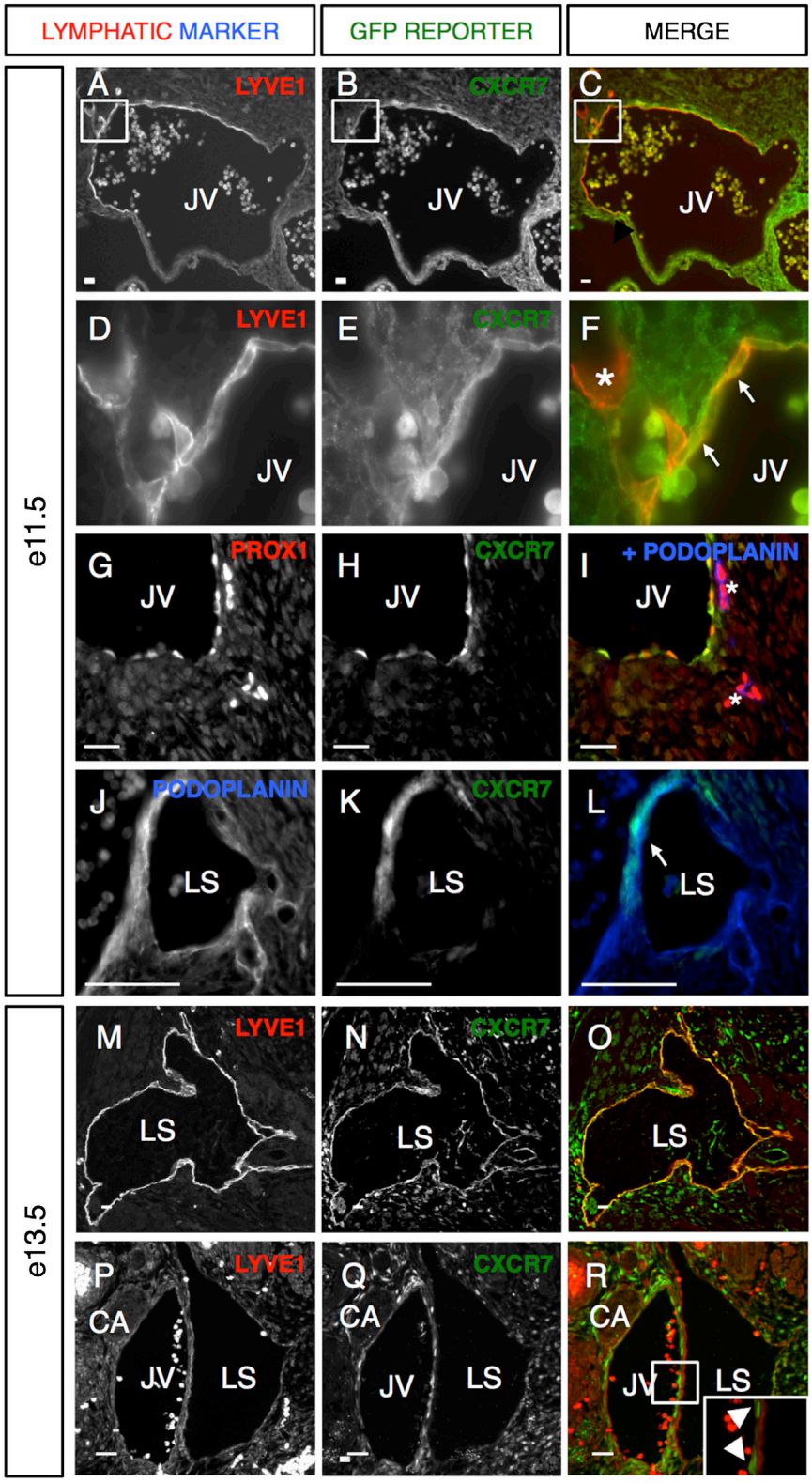

Figure 2. *Cxcr7* Is Dynamically Expressed in Lymphatic Endothelium during Development

(A–C) *Cxcr7* and LYVE1 colocalize in the JV of E11.5 *Cxcr7*$^{+/-}$ animals.

(D–F) Higher magnification of the LYVE1 positive portion of the JV. White arrows highlight areas of *Cxcr7* and LYVE1 colocalization. Asterisk highlights migrating LYVE1 positive, *Cxcr7* negative cells.

(G–I) *Cxcr7* and Prox1 colocalize in the JV of E11.5 *Cxcr7*$^{+/-}$ animals. Asterisks highlight migrating Prox1 positive, *Cxcr7* negative LECs.

(J–O) *Cxcr7* and lymphatic markers (J, podoplanin; M, LYVE1) colocalize in the LS (white arrows) of E11.5 (J)–(L) and E13.5 (M)–(O) *Cxcr7*$^{+/-}$ animals.

(P–R) *Cxcr7* is also expressed in cells of the JV directly adjacent to the LS. White arrowheads highlight *Cxcr7* expression in the JV. Scale bars represent 50 μM.

the jugular vein and precocious formation of enlarged, blood-filled lymph sacs (Figures S3C and S3D)—a process that typically occurs 1–2 days later in development. Thus, we reasoned that the likely cause of blood accumulation in the *Cxcr7*$^{-/-}$ mutants is precocious lymph sac formation prior to proper separation of the blood and lymphatic vascular systems.

Loss of CXCR7 Enhances LEC Migration In Vivo and In Vitro

We next sought to determine whether loss of *Cxcr7* affected lymphangiogenesis in other lymphatic vascular beds. At E18.5, staining of *Cxcr7*$^{-/-}$ cardiac tissue revealed increased LYVE1+ vessels on the surface of the heart (Figure 4A). This increase might be expected due to the cardiac hyperplasia in *Cxcr7*$^{-/-}$ embryos. Nevertheless, when normalized to total surface area of the heart, null animals exhibited a 20% increase in cardiac lymphatic vessels on the ventral surface of the heart (Figure 4B). Higher power examination of the cardiac lymphatic vessels of *Cxcr7*$^{-/-}$ animals revealed a disruption of branching complexity and lacunae number (Figures S4A–S4F), as well as an extensive network of lymphatic vessels in the curvature of the outflow tract on cardiac dorsal-surface (Figure S4C, arrows) that were not present in wild-type mice. Additionally, these LYVE1+ vessels tended to extend farther down the apex of the heart in *Cxcr7*$^{-/-}$ embryos, suggesting that *Cxcr7* also affects LEC migration (Figures 4A and 4C).

To elucidate whether loss of CXCR7 is directly involved in enhancing AM-mediated downstream signaling pathways and cellular migration, we utilized shRNA lentiviral vectors to achieve 80% knockdown of *CXCR7* in human LECs (Figure 4D). We first used a scavenger

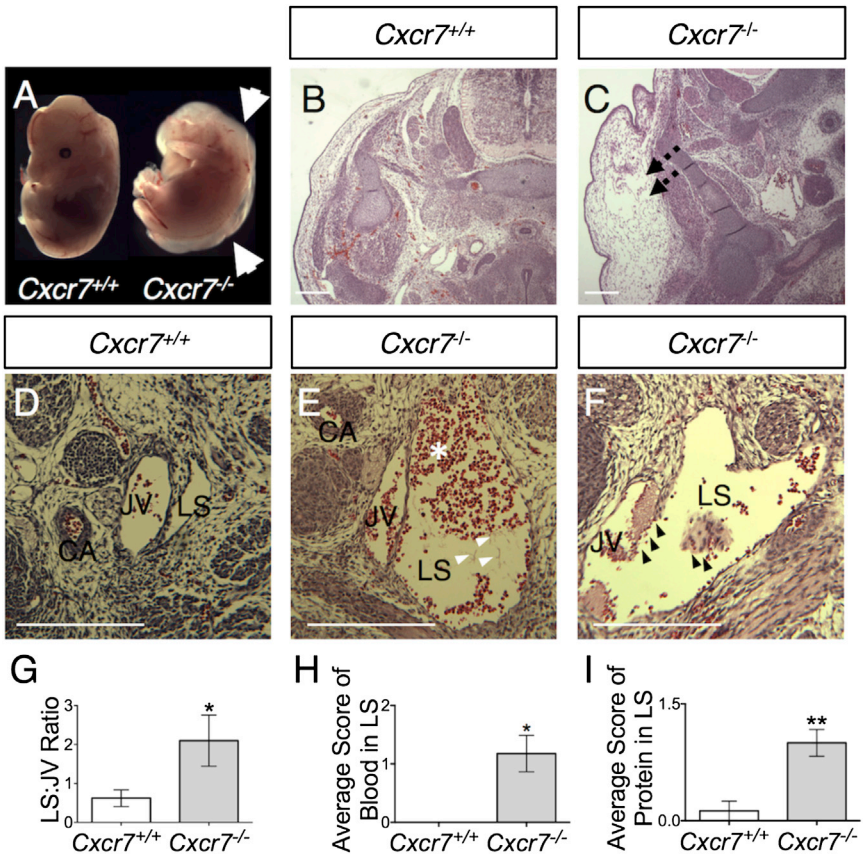

Figure 3. *Cxcr7*$^{-/-}$ Embryos Have Enlarged Blood-Filled Lymphatic Sacs and Interstitial Edema

(A–C) Some *Cxcr7*$^{-/-}$ embryos exhibit interstitial edema at E13.5 [white (A) and black (C) arrows].

(D–F) *Cxcr7*$^{-/-}$ embryos exhibit enlarged lymph sacs filled with blood (asterisks) and proteinaceous deposits (arrowheads) at E13.5. (F) In some *Cxcr7*$^{-/-}$ embryos, the LS fails to separate from the JV properly. Platelet thrombi are highlighted by arrowheads.

(G–I) Quantitation of the LS:JV ratio (t test) and blood and protein accumulation (Mann-Whitney U test) in the LS of *Cxcr7*$^{-/-}$ embryos (n = 10) compared to wild-type controls (n = 5). A detailed description of the scoring rubric is provided in the methods section. Data are represented as mean ± SEM. *$p < 0.05$, **$p < 0.01$.

See also Figure S3.

assay to confirm that *CXCR7* shRNA-infected LECs scavenged less AM than control cells, resulting in increased AM available to interact with the signaling receptor, CLR/R2 (Figures S5A and S5B). Next, we showed that knockdown of endogenous CXCR7 in LECs results in an increase in AM-mediated ERK phosphorylation, with *CXCR7* shRNA-infected LECs exhibiting a potent upregulation in pERK:tERK ratios in response to AM treatment, whereas control cells did not (Figure S5C).

These *CXCR7* knockdown cells were then used to evaluate whether loss of *CXCR7* enhances AM-mediated LEC migration. Using an in vitro scratch assay, we showed that AM promotes LEC migration, because AM-treated control cells migrated 41% more than vehicle-treated cells (Figures 4E and 4G). Furthermore, AM treatment of *CXCR7* knockdown cells caused the cells to migrate into the scratch 66% more than vehicle-treated cells (Figures 4F and 4H). Moreover, percent migration of AM-treated *CXCR7* knockdown LECs was significantly increased above all other conditions (Figure 4I). These scratch assay findings were fully recapitulated using a transwell migration assay (Figure 4J). Finally, the effect of CXCR7 on AM-mediated cell migration was corroborated using an overexpression model. As expected, AM treatment of CLR/RAMP2-expressing HEK293T cells resulted in increased migration across a transwell. However, this migration was abrogated when cells were cotransfected with a *CXCR7* expression plasmid (Figure 4K). Collectively, these data show that *CXCR7* expression modulates AM-mediated downstream signaling activity, with knockdown of endogenous *CXCR7* increasing and overexpression of *CXCR7* reducing AM-mediated cellular migration.

Dermal Lymphatic Vessels of *Cxcr7*$^{-/-}$ Animals Are Enlarged, with Less Branching Complexity

We also observed morphological changes in the dermal lymphatic vessels of *Cxcr7*$^{-/-}$ mice. Interestingly, although there was stochastic expression of *Cxcr7* in dermal lymphatic vessels (Figure S6), we consistently observed *Cxcr7* expression in blood vessels, again suggesting that non-cell-autonomous expression of *Cxcr7* can affect lymphangiogenesis. While the dermal lymphatics of wild-type animals formed a highly-structured lattice network, those of *Cxcr7*$^{-/-}$ embryos failed to extend and connect to neighboring vessels, resulting in fewer ring-like structures or lacunae (Figures 5A and 5B, asterisks). For example, control lymphatic capillary networks comprised between six to eight lacunae per image, but the lymphatic network of *Cxcr7*$^{-/-}$ skin consisted of only four to five lacunae per image (Figure 5C). Quantitation of the number of branch points also revealed a significant reduction in branching complexity, from 23.2 to 16.3 per image, between control and *Cxcr7*$^{-/-}$ dermal lymphatics (Figure 5D) (image area measured 132,800 μm^2). Additionally, *Cxcr7*$^{-/-}$ dermal lymphatic vessels were enlarged compared to littermate controls (Figures 5E–5I, yellow dashed line). The junctional area where vessels coalesce to form a branch point was also increased (Figures 5G, 5H, and 5J, yellow solid line).

Previously published studies demonstrate that this type of increase in vessel diameter and decreased branching complexity is consistent with a hyperplastic phenotype (Coxam et al., 2014; James et al., 2013), suggesting that loss of CXCR7 results in hyperproliferation of LECs. We therefore sought to determine if this hyperplastic phenotype of *Cxcr7*$^{-/-}$ dermal lymphatics could be attributed to increased AM-mediated LEC proliferation—a biological effect of AM which has been demonstrated by our group and others (Fritz-Six et al., 2008; Jin et al., 2008;

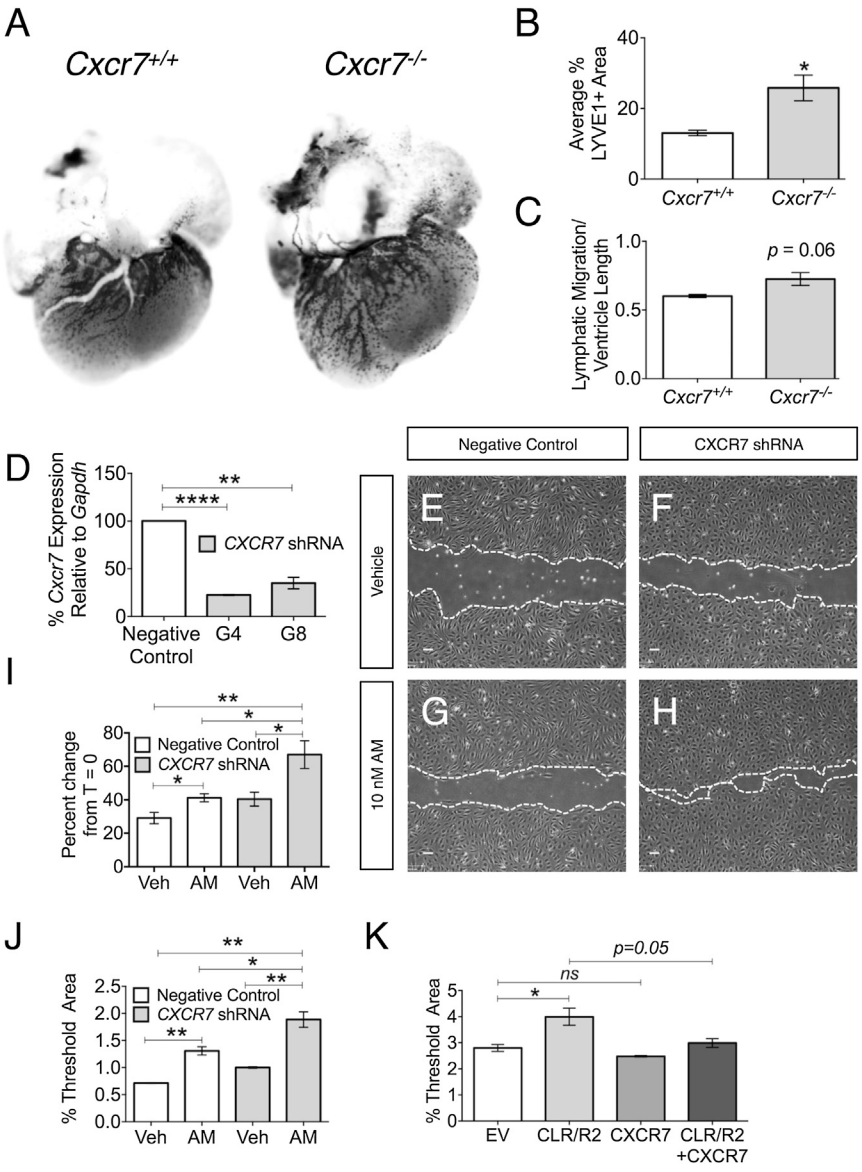

Figure 4. Loss of CXCR7 Enhances Cardiac Lymphangiogenesis by Promoting AM-Mediated Cellular Migration

(A) View of ventral side of whole mount hearts of E18.5 embryos stained with the lymphatic marker LYVE1.

(B and C) Quantitation of LYVE1 staining normalized to surface area (B) and LEC migration down the apex of the hearts (C) (n = 3).

(D) *CXCR7* knockdown in LECs by two shRNA lentiviral constructs.

(E–H) Control or *CXCR7* knockdown LECs treated with vehicle (E and F) or 10 nM AM at 18 hr (G and H). Migration from the time of scratch (T = 0) was measured. Scale bars represent 100 μM.

(I) Quantitation of LEC migration in *CXCR7* knockdown and control LECs.

(J and K) Quantitation of transwell migration of *CXCR7* knockdown LECs treated with vehicle or 10 nM AM (J), and empty vector (EV), CXCR7-, CLR/R2-, and CLR/R2+CXCR7-expressing HEK293T cells treated with 10 nM AM.

In (A)–(K), data are represented as mean ± SEM. *$p < 0.05$, **$p < 0.01$, ****$p < 0.001$. See also Figures S4 and S5.

Karpinich et al., 2013). Using *CXCR7* knockdown LECs, we observed a 50% increase in proliferation in AM-treated *CXCR7* knockdown LECs compared to AM-treated control cells (Figure 5K). Collectively, these data demonstrate that loss of CXCR7 promotes AM-mediated LEC lymphangiogenesis by enhancing both migration and proliferation in vivo and in vitro.

Genetic Titration of *Adm* Changes *Cxcr7*$^{-/-}$ Survival

We next sought to determine whether the phenotypes of *Cxcr7*$^{-/-}$ embryos could be causally associated with AM ligand concentration in vivo. To test this, we employed a genetic approach, depicted in Figures 6A and 6C, which allowed for the generation of *Cxcr7* gene-targeted mice on a titrated background of AM ligand that ranges from 50% to 300% wild-type levels. *Adm*$^{+/-}$ mice express 50% of wild-type levels of *Adm* mRNA and peptide and exhibit exacerbated cardiovascular damage, reduced female fertility, and defective lymphatic function (Caron and Smithies, 2001; Li et al., 2006; Nikitenko et al., 2013). *Adm*$^{hi/hi}$ animals survive to adulthood, but exhibit profound cardiac hyperplasia during development (Wetzel-Strong et al., 2014). Therefore, we were confident that the effective dosage of AM peptide achieved with the AM "gene titration" mice was within a range that would have significant biological impact on lymphatic and cardiac development.

First, because we noted some embryonic lethality in *Cxcr7*$^{-/-}$ animals in the genetic reduction experiment, we asked whether *Adm* haploinsufficiency might improve *Cxcr7*$^{-/-}$ embryo survival during midgestation. At E13.5 we observed equivalent numbers of *Cxcr7*$^{-/-}$;*Adm*$^{+/+}$ and *Cxcr7*$^{-/-}$;*Adm*$^{+/-}$ animals from compound heterozygous intercrosses (Figure 6B, E13.5). However, at E14.5 the expected 1:1 ratio of *Cxcr7*$^{-/-}$;*Adm*$^{+/+}$:*Cxcr7*$^{-/-}$;*Adm*$^{+/-}$ mice was significantly skewed, with <50% of the expected *Cxcr7*$^{-/-}$;*Adm*$^{+/+}$ genotype being offset by a disproportionate survival of *Cxcr7*$^{-/-}$;*Adm*$^{+/-}$ embryos (Figure 6B, E14.5). Thus, haploinsufficiency of *Adm* improves *Cxcr7*$^{-/-}$ embryo survival during midgestation. It is also noteworthy that embryonic lethality was significantly increased in the *Cxcr7*$^{+/-}$;*Adm*$^{+/-}$ cross, which is likely due to the critical role of AM in female reproductive physiology (Lenhart and Caron, 2012; Lenhart et al., 2014; Li et al., 2006, 2008, 2013). This finding suggests that disruption of the parental CXCR7-AM axis likely contributes to the severity of the phenotypes.

Next, we bred *Cxcr7*$^{+/-}$ mice to *Adm*$^{hi/hi}$ animals in order to evaluate whether AM overexpression might exacerbate *Cxcr7*$^{-/-}$ gestational loss or influence survival. Interestingly,

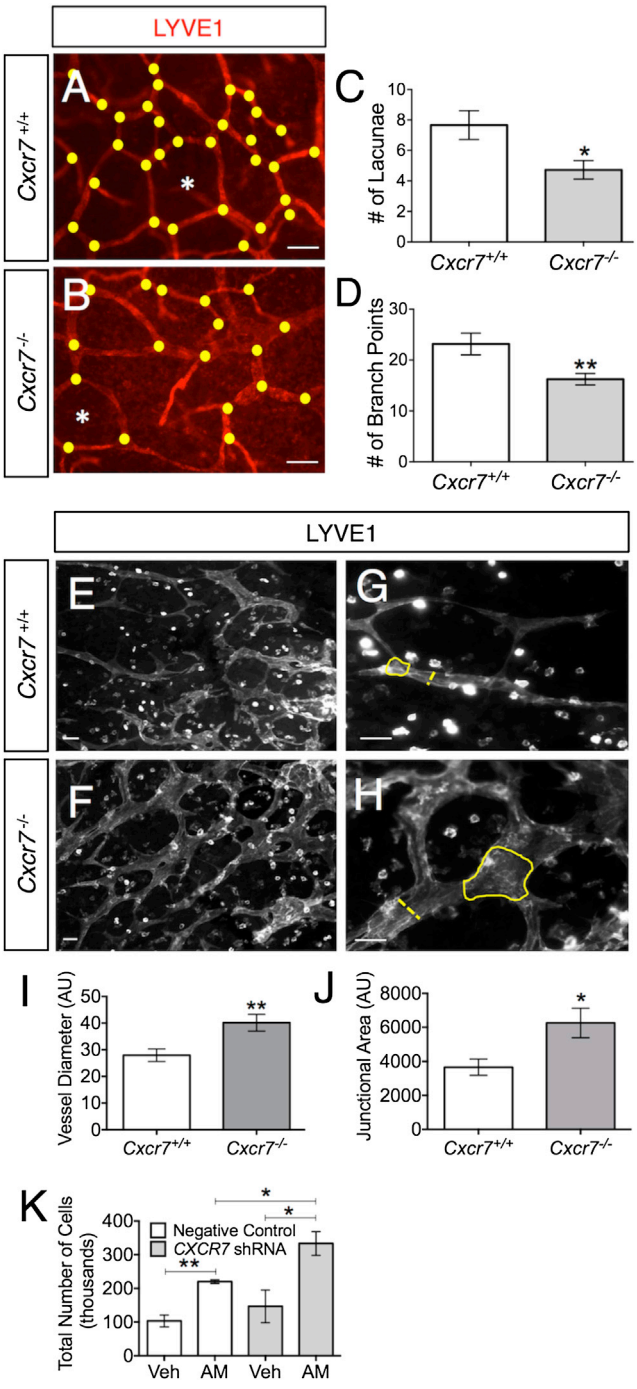

Figure 5. Loss of CXCR7 Causes Enlarged Dermal Lymphatics with Decreased Branching Complexity In Vivo and Enhances LEC Proliferation In Vitro

(A and B) *Cxcr7*$^{-/-}$ P1 skin (n = 5) exhibit dysmorphic dermal lymphangiogenesis compared to controls (n = 4). White asterisks identify a lacuna; yellow dots highlight branch points. Scale bars represent 50 μM.

(C and D) Quantitation of the number of lacunae and branch points respectively. Fewer lacunae and decreased branching complexity were observed in *Cxcr7*$^{-/-}$ animals. A branch point is defined as a vessel with three vessels branching away. A lacuna is defined as a space where three or more branch points coalesce.

(E–H) Skin of E13.5 *Cxcr7*$^{-/-}$ embryos. Scale bars represent 50 μM.

(I and J) Lymphatic vessels of P1 *Cxcr7*$^{-/-}$ embryos are dilated, with increased junctional area where vessels coalesce to form a branch point. Yellow dashed and straight line in (G) and (H) represent the vessel diameter and junctional area, respectively, measured in P1 skin.

(K) Quantitation of LEC proliferation after a 24 hr treatment with 10 nM AM.

In (A)–(K), data are represented as mean ± SEM. *p < 0.05, **p < 0.01. See also Figure S6.

we found that postnatal survival of compound heterozygous pups was poor, with ~30% postnatal lethality, making maintenance of the *Cxcr7*$^{+/-}$;*Adm*$^{hi/+}$ mouse colony very challenging. Whereas we had not previously observed *Cxcr7*$^{+/-}$ pup lethality in other genetic crosses, *Cxcr7*$^{+/-}$ animals that expressed a single *Adm*^{hi} allele were more susceptible to death. Moreover, homozygosity for the *Adm*^{hi} allele resulted in a striking 62% lethality of *Cxcr7*$^{+/-}$;*Adm*$^{hi/hi}$ mice (Figure 6D). Collectively, these data demonstrate that titration of the endogenous AM ligand is causally associated with profound changes in the survival of *Cxcr7* gene-targeted animals.

Haploinsufficiency of AM Normalizes Lymphatic and Cardiac Hyperproliferation of *Cxcr7*$^{-/-}$ Mice

Based on the improved embryonic survival of *Cxcr7*$^{-/-}$;*Adm*$^{+/-}$ embryos, we next performed phenotypic characterization of lymphatic and cardiac development in these animals, with the expectation that haploinsufficiency for AM ligand might normalize the hypertrophic cardiovascular phenotypes of *Cxcr7* null embryos. Importantly, haploinsufficiency for AM had no effect on the LS:JV ratio in *Cxcr7*$^{+/+}$ animals (Figures 6E and 6F). Consistent with Figures 3E–3G, the podoplanin-positive lymph sacs of E13.5 *Cxcr7*$^{-/-}$;*Adm*$^{+/+}$ embryos showed a significant 4-fold enlarged LS:JV ratio compared to wild-type littermates (Figures 6G and 6I). However, this lymph sac enlargement was normalized in *Cxcr7*$^{-/-}$;*Adm*$^{+/-}$ mice, resulting in LS:JV ratios that were statistically indistinguishable from wild-type animals (Figures 6H and 6I). Additionally, we used Ki67 staining to quantitate the number of proliferating LECs and found a direct correlation between the proliferation of LECs and the LS:JV ratios and genotypes. While *Cxcr7*$^{-/-}$;*Adm*$^{+/+}$ mice had significantly more proliferating cells in the LS compared to wild-type animals (Figures 6G and 6J), haploinsufficiency for AM (*Cxcr7*$^{-/-}$;*Adm*$^{+/-}$) allowed this hyperproliferation to revert to levels that were equivalent to those observed in wild-type animals (Figures 6H and 6J). Taken together, these findings demonstrate that the increase in LS:JV ratio in *Cxcr7* null mice is due to an increase in LEC proliferation that can be reversed by genetic reduction of AM ligand.

Similar effects were observed in the developing heart. Using BrdU incorporation assays, we quantitated the amount of proliferating cells in E11.5 cardiac tissue from the AM genetic titration animals. Percent proliferation of cardiac cells in *Cxcr7*$^{+/+}$;*Adm*$^{+/-}$ animals was equivalent to wild-type animals, demonstrating that *Adm* haploinsufficiency alone does not affect heart size (Figures 7A–7D). Consistent with other studies (Gerrits et al., 2008), we noted a statistically significant increase in proliferation of *Cxcr7*$^{-/-}$ cardiac tissue compared to wild-type (Figures 7E, 7F, and 7I). Importantly, this aberrant cardiac hyperproliferation was normalized to wild-type levels in *Cxcr7*$^{-/-}$;*Adm*$^{+/-}$ embryos (Figures 7G–7I). We noted increased proliferation particularly

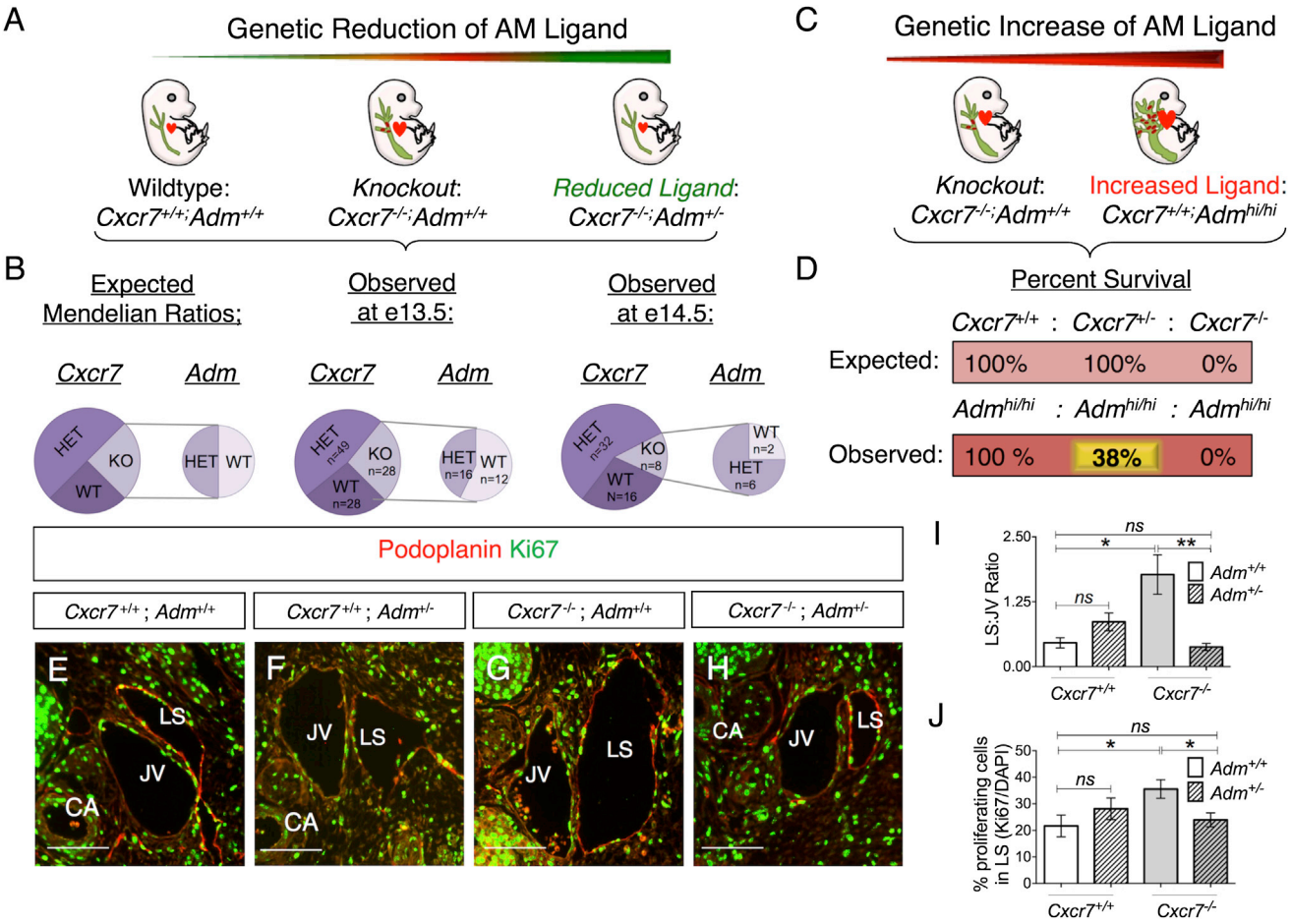

Figure 6. Genetic Titration of *Adm* Influences *Cxcr7*$^{-/-}$ Phenotypes

(A and B) Schematic of *Adm* genetic reduction experiment with expected and observed Mendelian ratios. *Cxcr7*$^{+/-}$;*Adm*$^{+/-}$ mice were bred with *Cxcr*$^{+/-}$;*Adm*$^{+/+}$ mice, resulting in the following expected distribution: 25% *Cxcr7*$^{+/+}$, 50% *Cxcr7*$^{+/-}$, and 25% *Cxcr7*$^{-/-}$ with 50% of each *Cxcr7* genotype being AM heterozygous. Observed number of animals (including resorptions) was statistically different from expected as judged by a χ^2 test ($p = 0.02$).

(C and D) Schematic of *Adm* genetic increase experiment with expected and observed percentage of survival of animals, n = 85. Observed number of animals was statistically different from expected as judged by a χ^2 test ($p = 0.001$).

(E–H) Representative images of JV and LS of E13.5 embryos from the gene reduction experiment stained for podoplanin and Ki67. Scale bars represent 100 μM.

(I) Quantitation of the LS:JV ratio in E13.5 embryos (n = 4–8 for each genotype).

(J) Percent proliferating cells in the LS (n = 4–8 for each genotype).

Data are represented as mean ± SEM. *$p < 0.05$, **$p < 0.01$ (one-way ANOVA).

within the epicardium and trabeculae (Figures 7F–7H, arrows and arrowheads, respectively)—regions of the heart where CXCR7 is highly expressed (see Figure 1F). Furthermore, 2 days after the AM-mediated peak in myocyte proliferation, many of the hearts of *Cxcr7*$^{-/-}$;*Adm*$^{+/-}$ embryos appeared phenotypically normal and similar in size to wild-type animals (Figures 7J–7L). We therefore conclude that genetic reduction of AM peptide alleviates the pathological cardiac hyperproliferation of *Cxcr7* null animals and ultimately impacts cardiac size during development.

Although difficulty maintaining the line precluded extensive timed matings, we observed even more precocious development of the LS of *Cxcr7*$^{-/-}$;*Adm*$^{hi/hi}$ embryos. At E11.5, *Cxcr7*$^{-/-}$;*Adm*$^{hi/hi}$ embryos often had fully formed lymph sacs that were dramatically enlarged and blood-filled (Figure S3E). This further exacerbated lymphatic development confirmed our hypothesis that *Cxcr7*$^{-/-}$ LS develop precociously. Hearts of *Cxcr7*$^{-/-}$ on the *Adm*$^{hi/hi}$ background also tended to be enlarged with thickened compact zones and significant blood accumulation in the ventricles and atria (data not shown).

DISCUSSION

The pleiotropic consequences of CXCR7 loss have made it difficult to discern which ligand(s) are responsible for a given phenotype. In this study, using both loss-of-function and gain-of-function animal models, we demonstrate that several of the essential functions of CXCR7 during cardiovascular development can be attributed to its decoy activities for the ligand AM. Haploinsufficiency of AM in a *Cxcr7*$^{-/-}$ animal effectively reversed cardiac and lymphatic hyperproliferation, demonstrating that CXCR7 is required as a molecular rheostat for

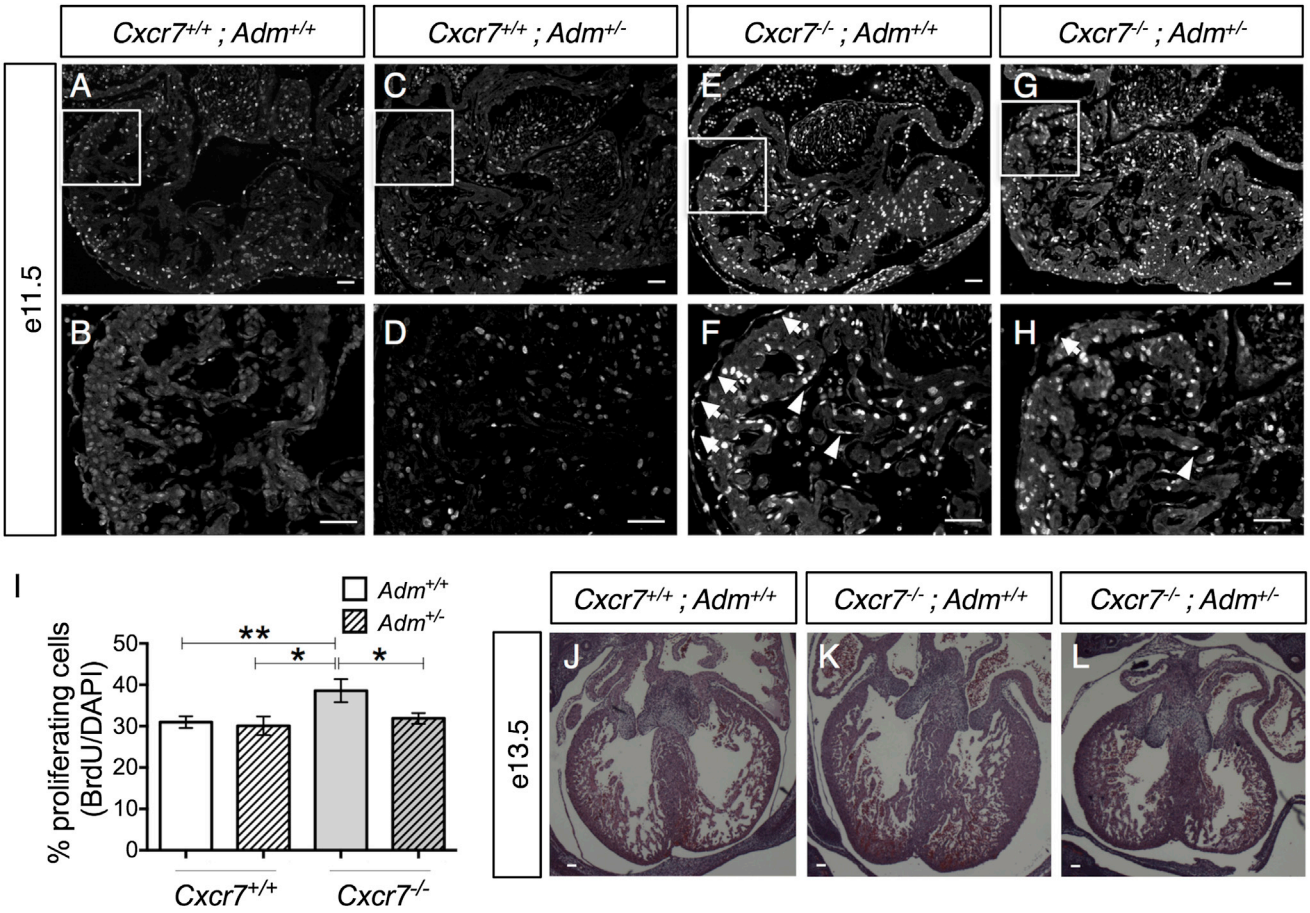

Figure 7. Genetic Reduction of *Adm* Normalizes *Cxcr7*$^{-/-}$ Cardiac Proliferation and Size

(A–G) (A, C, E, and G): BrdU staining of cardiac tissue of E11.5 embryos from the gene titration experiment. Exposure, 750 ms. Scale bars represent 100 μM. (B, D, F, and H): arrows highlight proliferating epicardium, and arrowheads highlight proliferating endocardium. Exposure, 250 ms. Scale bars represent 100 μM.

(I) Percent proliferating cardiac cells in embryos from genetic reduction experiment (n = 3–5 for each genotype). Data are represented as mean ± SEM. *p < 0.05 (one-way ANOVA).

(J–L) H&E-stained cardiac tissue of E13.5 animals from the genetic reduction experiment (n = 3–5 for each genotype). Scale bars represent 100 μM.

controlling AM ligand availability during development. While other atypical chemokine receptors are known to bind multiple ligands, only recently has the repertoire of CXCR7 ligands been expanded beyond the chemokines CXCL12 and CXCL11. For example, a very recent study has elegantly demonstrated that proteolytic peptide fragments of the adrenal neuropeptide proenkaphalin A interact with CXCR7 and thereby mediate responses to glucocorticoid secretion and anxiety behaviors in mice (Ikeda et al., 2013). Structure-function studies of the proenkaphalin A-derived peptides, along with our current findings on the AM peptide, further highlight the ability of CXCR7 to bind to several classes of small peptidergic ligands, which also happen to be particularly enriched in the adrenal gland. Whether adrenomedullin—which as it name implies, is also highly expressed in the adrenal gland—is also implicated in the CXCR7-mediated glucocorticoid secretion and anxiety behaviors has yet to be determined.

Likewise, our study does not formally rule out the involvement of CXCL12 in the described cardiovascular hyperplasia phenotypes of *Cxcr7*$^{-/-}$ mice. Genetic deletion of either CXCR4 or CXCL12 has been associated with defective ventricular septum formation (Ma et al., 1998; Zou et al., 1998). However, only recently have studies in chick embryos demonstrated a gain-of-function phenotype for CXCL12 overexpression in neural crest cell migration related to cardiac development (Escot et al., 2013). While the effects of CXCL12 overexpression might be anticipated to more closely parallel the effects of CXCR7 loss-of-function, the cardiac phenotypes of these two models are markedly different. CXCL12 misexpression in chick embryos diverts neural crest cell migration to the heart, while CXCR7 deficiency promotes cardiac myocyte hyperplasia and septal defects. Our current study does not preclude the functional deregulation of CXCL12, however, it does definitively demonstrate that genetic reduction in AM ligand is fully sufficient to rescue the *Cxcr7*$^{-/-}$ cardiac hyperplasia. Therefore, although we cannot exclude potential effects of CXCL12 on the *Cxcr7*$^{-/-}$ cardiac phenotypes, we have identified AM as the critical ligand for mediating the cardiac hyperproliferation.

With respect to lymphangiogenesis, genetic studies in zebrafish have also established a central role for CXCL12(SDF-1)/CXCR4

signaling during the stepwise assembly of the lymphatic trunk network (Cha et al., 2012). Interestingly, the requirement for CXCL12 in guiding zebrafish LEC migration occurs at developmental time points that are subsequent to LEC sprouting from the posterior cardinal vein. However, our expression studies in mice revealed little expression of CXCR7 in LECs that have migrated away from the jugular vein, and we failed to observe prominent defects in the migration and assembly of lymphatic sacs in *Cxcr7*$^{-/-}$ mice. Although these spatiotemporal differences in receptor-ligand expression patterns may simply be attributed to differences between species, a more compelling implication of these studies is that dynamic changes in the expression of CXCR4 and CXCR7 may be critical for orchestrating the extent and time frame to which nascent LECs sense and respond to different lymphangiogenic growth factors. Moreover, the dynamic spatiotemporal expression of signaling and decoy receptors likely provides a mechanism for individual LECs and their adjacent tissues to create a localized microgradient of chemotactic or proliferative factors (Donà et al., 2013; Venkiteswaran et al., 2013) to promote the stepwise growth of lymphatic vessels.

Although our current study has focused on the effects of CXCR7 on AM-mediated cardiac and lymphatic development, it is important to recognize that the interaction of CXCR7 with AM may initiate downstream signaling and active processes in other cell types or tissues. For example, several studies have pointed to potential nondecoy functions of CXCR7, such as signaling through β-arrestin, heterodimerizing with other GPCRs in certain tissues, and coupling with G-proteins in astrocytes (Kapas and Clark, 1995; Odemis et al., 2012; Rajagopal et al., 2010). Therefore, while we have currently established CXCR7 as a molecular rheostat for AM signaling during cardiovascular development, future studies may identify potential CXCR7-GPCR complexes that allow for functional AM signaling in other cell types or tissues.

Our findings of increased ERK phosphorylation in dermal lymphatics of *Cxcr7*$^{-/-}$ mice are consistent with several previously described models with aberrant lymphangiogenesis associated with increased ERK signaling. For example, ex vivo expression of *Spred-1/2*, negative regulators of ERK activation, suppresses LEC proliferation while double knockout mice exhibit dilated, blood-filled lymphatics—similar to the *Cxcr7*$^{-/-}$ phenotype described by Taniguchi et al. (2007). Likewise, mice lacking *apoptosis stimulating protein of p53* (*Aspp1*) have increased ERK activation and exhibit similar transient subcutaneous edema with dilated and dysmorphic lymphatics and increases in cardiac LYVE1+ staining (Hirashima et al., 2008). Most recently, a fine-tuned balance between ERK and Akt signaling pathways has been recognized as an essential component for establishing LEC fate determination and differentiation (Deng et al., 2013; Simons and Eichmann, 2013). Collectively, these studies identify ERK signaling as a critical regulator of lymphangiogenesis and either loss or excessive ERK signal as a cause of aberrant lymphangiogenesis. Results of this study identify a mechanism, whereby the positioning of a decoy receptor at the junction of lymphatic sprouting and migration serves as a biological rheostat for regulating the migratory and mitogenic effects of lymphangiogenic growth factors that are upstream of ERK activation. Additional studies to determine whether and how other atypical chemokine receptors may influence cardiac and lymphatic development are warranted and may lead to conceptual paradigms about how growth factor gradients and their downstream signaling pathways can be precisely controlled by 7-transmembrane decoy receptors during cardiovascular development.

EXPERIMENTAL PROCEDURES

Mice

Mice that contain a GFP reporter knocked into the *Cxcr7* gene were purchased (C57BL/6-*Ackr3*^{tm1Litt}/J, Jackson Laboratory). Generation of *Adm*$^{+/-}$ and *Adm*$^{hi/hi}$ mice with a targeted, deletion and overexpression of *Adm,* respectively, has been previously described (Caron and Smithies, 2001; Dackor et al., 2006; Li et al., 2013). For timed pregnancies, *Cxcr7*$^{+/-}$ animals were intercrossed with *Cxcr7*$^{+/-}$ or *Cxcr7*$^{+/-}$;*Adm*$^{+/-}$ animals. Dams were monitored for vaginal plugs, and the day when the vaginal plug was detected was considered E0.5. *Cxcr7*$^{+/-}$;*Adm*$^{hi/+}$ animals were also intercrossed to establish survival. For BrdU incorporation assays, pregnant females were injected with BrdU (0.1 mg/g of BW, Sigma-Aldrich) via intraperitoneal injection 2 hr prior to dissection. All experiments involving mice were approved by the Institutional Animal Care and Use Committee at The University of North Carolina at Chapel Hill.

Cell Culture and RNAi

Human adult (HMVECdLyAd-Der) and neonatal (HMVEC-d Neo) dermal lymphatic endothelial cells (Lonza) were cultured in EGM-2MV media. HEK293T cells were maintained in DMEM with 10% fetal bovine serum and 1% penicillin streptomycin or gentamicin. Lentiviral particle production and infection were performed according to standard protocol. Briefly, human *CXCR7* shRNA pLKO1 vectors (UNC Viral Core) were cotransfected into HEK293T cells with lentiviral packaging vectors psPAX2 and MD2.G (Addgene) using Lipofectamine 2000 (Invitrogen). Viral supernatants were filtered, supplemented with 6 μg/ml polybrene, and used to infect LECs for 48 hr before functional assays were performed.

Gene Expression Analysis

Agilent human gene expression microarrays were performed on three independent plates of hLECs treated with 10 nM AM (American Peptide). Analysis was performed using the Significance Analysis of Microarrays (SAM) software (Stanford University). For embryonic endothelial cells, CD31 positive cells were isolated using magnetic beads. Quantitative RT-PCR was performed using primers and probes or *hCXCR7* Assays on Demand (Life Technology) after reverse transcription of 2 μg of total RNA. For AM_{22-52} treatment, cells were incubated with 1 μM AM_{22-52} (American Peptide Company) for 30 min prior to treatment with 10 nM AM and 1 μM AM_{22-52}.

Scavenger Assay

HEK293T cells were transfected with *CXCR7* or pcDNA3.1 (negative control) using standard calcium phosphate transfection. Cells were treated with biotinylated-AM (Phoenix Pharmaceuticals), and aliquots of media were collected over 8 hr. Biotinylated-AM was detected with IRDye Streptavidin (1:2,500, Li-COR).

ERK Phosphorylation

HEK293T cells were transfected with expression plasmids, serum-starved for 20 hr, and treated with vehicle or 10 nM AM for 1 min. Blots were blocked in 5% BSA, probed overnight with monoclonal rabbit anti-mouse pERK and tERK (1:1000, Cell Signaling) and monoclonal mouse anti-GAPDH (1:2000, Novus Biologicals), incubated in appropriate secondary antibody, and imaged on the Odyssey scanner (Li-COR). A blot with three independent experiments run on the same gel was used to perform statistical analysis.

Immunohistochemistry

Embryo sections and whole mount tissue were permeabilized, blocked with 5% normal donkey serum, and incubated overnight at room temperature with primary antibodies, and then probed with appropriate secondary antibodies. Antibodies are described in the Supplemental Experimental Procedures.

Quantitation of LS:JV Ratio and Blood and Protein Accumulation in LS

Transverse sections of jugular lymph sacs of wild-type and mutant mice were hematoxylin and eosin (H&E) stained. The area of the LS and JV were measured using ImageJ software (NIH), and sections were graded for blood and protein accumulation in the LS using a scoring rubric. Blood and protein were graded as follows: 0 = no red blood cells (RBC); 1 = 3–10 RBC; 2 = 3–50 RBCs; 3 = >50 RBCs; 0 = no protein; 1 = minimal protein accumulation; 2 = moderate protein accumulation; 3 = extensive protein accumulation. Brightfield images were taken on a Leitz Dialux 20 Microscope.

In Vitro Migration and Proliferation Assays

Scratch Assay

CXCR7 knockdown (and negative control) LECs were grown to confluence and then scratched with a pipette tip. LECs were rinsed with PBS to remove nonadherent cells and then treated in 0.5% FBS RPMI with vehicle or 10 nM AM. Four fields per well were imaged at T = 0 hr and at T = 18 hr postscratch using an Olympus IX-81 inverted microscope equipped with a QImaging Retiga 4000R camera at 4× magnification. The percent change in migration was calculated by measuring the open area of the scratch (ImageJ). Results shown are representative of three independent experiments.

Transwell Migration Assay

HEK293T cells transfected with expression plasmids and LECs with lentiviral-induced *CXCR7* knockdown were labeled with 5 μM Cell Tracker Green (CTG) CMFDA (Life Technologies). Cells (1×10^5) were treated with 10 nM AM for 5 min and then seeded onto 8 μm transwell inserts (BD Biosciences). After 4 hr incubation, inserts were fixed with 4% PFA, and filters were mounted for analysis. Quantitation of transmigrated cells was done by measuring the threshold of CTG-labeled cell fluorescence using ImageJ (NIH).

Proliferation

CXCR7 knockdown and control LECs were plated, serum starved for 4 hr, then treated with 10 nM AM for 24 hr. Cells counts were assessed using a Countess Automated Cell counter (Life Technology).

Statistical Analysis

Student's two-tailed t test was used for all comparisons unless otherwise noted in the corresponding figure legend.

ACCESSION NUMBERS

The Gene Expression Omnibus (GEO) accession number for the microarray reported in this paper is GSE59938.

SUPPLEMENTAL INFORMATION

Supplemental Information includes Supplemental Experimental Procedures, six figures, and one table and can be found with this article online at http://dx.doi.org/10.1016/j.devcel.2014.07.012.

ACKNOWLEDGMENTS

The authors thank Dr. Nikolaus Heveker, University of Montreal, for his helpful discussions and insights. We also thank former members of the K.M.C. laboratory, including Kimberly Fritz-Six, Drs. Manyu Li, Mahita Kadmiel, and Patricia Lenhart, and Kirk McNaughton and Ashley Ezzell of the Histopathology Core for their assistance with experiments and technical guidance. This work was supported by funds from the American Heart Association EIA (0555424U) and NIH grants (HD060860 and DK099156 to K.M.C.), F30 HL118932 (to K.R.K.), and training grants HL069768 and GM008719.

Received: February 21, 2014
Revised: June 6, 2014
Accepted: July 14, 2014
Published: September 8, 2014

REFERENCES

Barak, L.S., Salahpour, A., Zhang, X., Masri, B., Sotnikova, T.D., Ramsey, A.J., Violin, J.D., Lefkowitz, R.J., Caron, M.G., and Gainetdinov, R.R. (2008). Pharmacological characterization of membrane-expressed human trace amine-associated receptor 1 (TAAR1) by a bioluminescence resonance energy transfer cAMP biosensor. Mol. Pharmacol. *74*, 585–594.

Berahovich, R.D., Zabel, B.A., Lewén, S., Walters, M.J., Ebsworth, K., Wang, Y., Jaen, J.C., and Schall, T.J. (2014). Endothelial expression of CXCR7 and the regulation of systemic CXCL12 levels. Immunology *141*, 111–122.

Bertozzi, C.C., Schmaier, A.A., Mericko, P., Hess, P.R., Zou, Z., Chen, M., Chen, C.Y., Xu, B., Lu, M.M., Zhou, D., et al. (2010). Platelets regulate lymphatic vascular development through CLEC-2-SLP-76 signaling. Blood *116*, 661–670.

Boldajipour, B., Mahabaleshwar, H., Kardash, E., Reichman-Fried, M., Blaser, H., Minina, S., Wilson, D., Xu, Q., and Raz, E. (2008). Control of chemokine-guided cell migration by ligand sequestration. Cell *132*, 463–473.

Caron, K.M., and Smithies, O. (2001). Extreme hydrops fetalis and cardiovascular abnormalities in mice lacking a functional Adrenomedullin gene. Proc. Natl. Acad. Sci. USA *98*, 615–619.

Cha, Y.R., Fujita, M., Butler, M., Isogai, S., Kochhan, E., Siekmann, A.F., and Weinstein, B.M. (2012). Chemokine signaling directs trunk lymphatic network formation along the preexisting blood vasculature. Dev. Cell *22*, 824–836.

Coxam, B., Sabine, A., Bower, N.I., Smith, K.A., Pichol-Thievend, C., Skoczylas, R., Astin, J.W., Frampton, E., Jaquet, M., Crosier, P.S., et al. (2014). Pkd1 regulates lymphatic vascular morphogenesis during development. Cell Reports *7*, 623–633.

Dackor, R.T., Fritz-Six, K., Dunworth, W.P., Gibbons, C.L., Smithies, O., and Caron, K.M. (2006). Hydrops fetalis, cardiovascular defects, and embryonic lethality in mice lacking the calcitonin receptor-like receptor gene. Mol. Cell. Biol. *26*, 2511–2518.

Dambly-Chaudière, C., Cubedo, N., and Ghysen, A. (2007). Control of cell migration in the development of the posterior lateral line: antagonistic interactions between the chemokine receptors CXCR4 and CXCR7/RDC1. BMC Dev. Biol. *7*, 23.

Deng, Y., Atri, D., Eichmann, A., and Simons, M. (2013). Endothelial ERK signaling controls lymphatic fate specification. J. Clin. Invest. *123*, 1202–1215.

Donà, E., Barry, J.D., Valentin, G., Quirin, C., Khmelinskii, A., Kunze, A., Durdu, S., Newton, L.R., Fernandez-Minan, A., Huber, W., et al. (2013). Directional tissue migration through a self-generated chemokine gradient. Nature *503*, 285–289.

Duda, D.G., Kozin, S.V., Kirkpatrick, N.D., Xu, L., Fukumura, D., and Jain, R.K. (2011). CXCL12 (SDF1alpha)-CXCR4/CXCR7 pathway inhibition: an emerging sensitizer for anticancer therapies? Clin. Cancer Res. *17*, 2074–2080.

Dunworth, W.P., Fritz-Six, K.L., and Caron, K.M. (2008). Adrenomedullin stabilizes the lymphatic endothelial barrier in vitro and in vivo. Peptides *29*, 2243–2249.

Escot, S., Blavet, C., Härtle, S., Duband, J.L., and Fournier-Thibault, C. (2013). Misregulation of SDF1-CXCR4 signaling impairs early cardiac neural crest cell migration leading to conotruncal defects. Circ. Res. *113*, 505–516.

Fritz-Six, K.L., Dunworth, W.P., Li, M., and Caron, K.M. (2008). Adrenomedullin signaling is necessary for murine lymphatic vascular development. J. Clin. Invest. *118*, 40–50.

Gerrits, H., van Ingen Schenau, D.S., Bakker, N.E., van Disseldorp, A.J., Strik, A., Hermens, L.S., Koenen, T.B., Krajnc-Franken, M.A., and Gossen, J.A. (2008). Early postnatal lethality and cardiovascular defects in CXCR7-deficient mice. Genesis *46*, 235–245.

Graham, G.J., Locati, M., Mantovani, A., Rot, A., and Thelen, M. (2012). The biochemistry and biology of the atypical chemokine receptors. Immunol. Lett. *145*, 30–38.

Hirashima, M., Sano, K., Morisada, T., Murakami, K., Rossant, J., and Suda, T. (2008). Lymphatic vessel assembly is impaired in Aspp1-deficient mouse embryos. Dev. Biol. *316*, 149–159.

Hoopes, S.L., Willcockson, H.H., and Caron, K.M. (2012). Characteristics of multi-organ lymphangiectasia resulting from temporal deletion of calcitonin receptor-like receptor in adult mice. PLoS ONE *7*, e45261.

Ikeda, Y., Kumagai, H., Skach, A., Sato, M., and Yanagisawa, M. (2013). Modulation of circadian glucocorticoid oscillation via adrenal opioid-CXCR7 signaling alters emotional behavior. Cell *155*, 1323–1336.

James, J.M., Nalbandian, A., and Mukouyama, Y.S. (2013). TGFβ signaling is required for sprouting lymphangiogenesis during lymphatic network development in the skin. Development *140*, 3903–3914.

Jin, D., Harada, K., Ohnishi, S., Yamahara, K., Kangawa, K., and Nagaya, N. (2008). Adrenomedullin induces lymphangiogenesis and ameliorates secondary lymphoedema. Cardiovasc. Res. *80*, 339–345.

Kapas, S., and Clark, A.J. (1995). Identification of an orphan receptor gene as a type 1 calcitonin gene-related peptide receptor. Biochem. Biophys. Res. Commun. *217*, 832–838.

Karpinich, N.O., Hoopes, S.L., Kechele, D.O., Lenhart, P.M., and Caron, K.M. (2011). Adrenomedullin function in vascular endothelial cells: insights from genetic mouse models. Curr. Hypertens. Rep. *7*, 228–239.

Karpinich, N.O., Kechele, D.O., Espenschied, S.T., Willcockson, H.H., Fedoriw, Y., and Caron, K.M. (2013). Adrenomedullin gene dosage correlates with tumor and lymph node lymphangiogenesis. FASEB J. *27*, 590–600.

Lenhart, P.M., and Caron, K.M. (2012). Adrenomedullin and pregnancy: perspectives from animal models to humans. Trends Endocrinol. Metab. *23*, 524–532.

Lenhart, P.M., Nguyen, T., Wise, A., Caron, K.M., Herring, A.H., and Stuebe, A.M. (2014). Adrenomedullin signaling pathway polymorphisms and adverse pregnancy outcomes. Am. J. Perinatol. *31*, 327–334.

Li, M., Yee, D., Magnuson, T.R., Smithies, O., and Caron, K.M. (2006). Reduced maternal expression of adrenomedullin disrupts fertility, placentation, and fetal growth in mice. J. Clin. Invest. *116*, 2653–2662.

Li, M., Wu, Y., and Caron, K.M. (2008). Haploinsufficiency for adrenomedullin reduces pinopodes and diminishes uterine receptivity in mice. Biol. Reprod. *79*, 1169–1175.

Li, M., Schwerbrock, N.M., Lenhart, P.M., Fritz-Six, K.L., Kadmiel, M., Christine, K.S., Kraus, D.M., Espenschied, S.T., Willcockson, H.H., Mack, C.P., and Caron, K.M. (2013). Fetal-derived adrenomedullin mediates the innate immune milieu of the placenta. J. Clin. Invest. *123*, 2408–2420.

Ma, Q., Jones, D., Borghesani, P.R., Segal, R.A., Nagasawa, T., Kishimoto, T., Bronson, R.T., and Springer, T.A. (1998). Impaired B-lymphopoiesis, myelopoiesis, and derailed cerebellar neuron migration in CXCR4- and SDF-1-deficient mice. Proc. Natl. Acad. Sci. USA *95*, 9448–9453.

Moissoglu, K., Majumdar, R., and Parent, C.A. (2014). Cell migration: sinking in a gradient. Curr. Biol. *24*, R23–R25.

Murtomaki, A., Uh, M.K., Choi, Y.K., Kitajewski, C., Borisenko, V., Kitajewski, J., and Shawber, C.J. (2013). Notch1 functions as a negative regulator of lymphatic endothelial cell differentiation in the venous endothelium. Development *140*, 2365–2376.

Naumann, U., Cameroni, E., Pruenster, M., Mahabaleshwar, H., Raz, E., Zerwes, H.G., Rot, A., and Thelen, M. (2010). CXCR7 functions as a scavenger for CXCL12 and CXCL11. PLoS ONE *5*, e9175.

Neusser, M.A., Kraus, A.K., Regele, H., Cohen, C.D., Fehr, T., Kerjaschki, D., Wüthrich, R.P., Penfold, M.E., Schall, T., and Segerer, S. (2010). The chemokine receptor CXCR7 is expressed on lymphatic endothelial cells during renal allograft rejection. Kidney Int. *77*, 801–808.

Nibbs, R.J., and Graham, G.J. (2013). Immune regulation by atypical chemokine receptors. Nat. Rev. Immunol. *13*, 815–829.

Nikitenko, L.L., Shimosawa, T., Henderson, S., Mäkinen, T., Shimosawa, H., Qureshi, U., Pedley, R.B., Rees, M.C., Fujita, T., and Boshoff, C. (2013). Adrenomedullin haploinsufficiency predisposes to secondary lymphedema. J. Invest. Dermatol. *133*, 1768–1776.

Odemis, V., Lipfert, J., Kraft, R., Hajek, P., Abraham, G., Hattermann, K., Mentlein, R., and Engele, J. (2012). The presumed atypical chemokine receptor CXCR7 signals through G(i/o) proteins in primary rodent astrocytes and human glioma cells. Glia *60*, 372–381.

Ponimaskin, E.G., Heine, M., Zeug, A., Voyno-Yasenetskaya, T., and Salonikidis, P.S. (2007). Monitoring receptor-mediated changes of intracellular cAMP level by using ion channels and fluorescent proteins as biosensors. In Serotonin Receptors in Neurobiology, A. Chattopadhyay, ed. (Boca Raton: CRC Press), pp. 19–40.

Rajagopal, S., Kim, J., Ahn, S., Craig, S., Lam, C.M., Gerard, N.P., Gerard, C., and Lefkowitz, R.J. (2010). Beta-arrestin- but not G protein-mediated signaling by the "decoy" receptor CXCR7. Proc. Natl. Acad. Sci. USA *107*, 628–632.

Sánchez-Alcañiz, J.A., Haege, S., Mueller, W., Pla, R., Mackay, F., Schulz, S., López-Bendito, G., Stumm, R., and Marín, O. (2011). Cxcr7 controls neuronal migration by regulating chemokine responsiveness. Neuron *69*, 77–90.

Sánchez-Martín, L., Sánchez-Mateos, P., and Cabañas, C. (2013). CXCR7 impact on CXCL12 biology and disease. Trends Mol. Med. *19*, 12–22.

Sierro, F., Biben, C., Martínez-Muñoz, L., Mellado, M., Ransohoff, R.M., Li, M., Woehl, B., Leung, H., Groom, J., Batten, M., et al. (2007). Disrupted cardiac development but normal hematopoiesis in mice deficient in the second CXCL12/SDF-1 receptor, CXCR7. Proc. Natl. Acad. Sci. USA *104*, 14759–14764.

Simons, M., and Eichmann, A. (2013). Physiology. Lymphatics are in my veins. Science *341*, 622–624.

Taniguchi, K., Kohno, R., Ayada, T., Kato, R., Ichiyama, K., Morisada, T., Oike, Y., Yonemitsu, Y., Maehara, Y., and Yoshimura, A. (2007). Spreds are essential for embryonic lymphangiogenesis by regulating vascular endothelial growth factor receptor 3 signaling. Mol. Cell. Biol. *27*, 4541–4550.

Thelen, M., and Thelen, S. (2008). CXCR7, CXCR4 and CXCL12: an eccentric trio? J. Neuroimmunol. *198*, 9–13.

Valentin, G., Haas, P., and Gilmour, D. (2007). The chemokine SDF1a coordinates tissue migration through the spatially restricted activation of Cxcr7 and Cxcr4b. Curr. Biol. *17*, 1026–1031.

Venkiteswaran, G., Lewellis, S.W., Wang, J., Reynolds, E., Nicholson, C., and Knaut, H. (2013). Generation and dynamics of an endogenous, self-generated signaling gradient across a migrating tissue. Cell *155*, 674–687.

Wang, Y., Li, G., Stanco, A., Long, J.E., Crawford, D., Potter, G.B., Pleasure, S.J., Behrens, T., and Rubenstein, J.L. (2011). CXCR4 and CXCR7 have distinct functions in regulating interneuron migration. Neuron *69*, 61–76.

Wetzel-Strong, S.E., Li, M., Klein, K.R., Nishikimi, T., and Caron, K.M. (2014). Epicardial-derived adrenomedullin drives cardiac hyperplasia during embryogenesis. Dev. Dyn. *243*, 243–256.

Yu, S., Crawford, D., Tsuchihashi, T., Behrens, T.W., and Srivastava, D. (2011). The chemokine receptor CXCR7 functions to regulate cardiac valve remodeling. Dev. Dyn. *240*, 384–393.

Zou, Y.R., Kottmann, A.H., Kuroda, M., Taniuchi, I., and Littman, D.R. (1998). Function of the chemokine receptor CXCR4 in haematopoiesis and in cerebellar development. Nature *393*, 595–599.